ACS APPLIED MATERIALS & INTERFACES

Research Article

www.acsami.org

Electrocatalytic Properties of Hollow Coral-like Platinum Mesocrystals

Tian Li, Hongjun You,* Minwei Xu, Xiaoping Song, and Jixiang Fang*

School of Science, MOE Key Laboratory for Nonequilibrium Synthesis and Modulation of Condensed Matter, Xi'an Jiaotong University, Shaan Xi 710049, P. R. China

ABSTRACT: Controlling the morphology and size of Pt nanostructures can provide a great opportunity to improve their electrocatalytic properties and durability toward methanol oxidation. We successfully synthesized well-defined hollow coral-like Pt mesocrystals via a facile replacement reaction, using hierarchically structured Ag nanoparticles as the template. The as-synthesized coral-like Pt mesocrystals had hollow structures composed of porous walls that were 5−7 nm thick, which were constructed from numerous pores (~2 nm) and small (~5 nm) Pt nanoparticle building units. These hollow and porous structures exhibited large electrochemical surface areas. The Pt mesostructures that have single-crystal inherence as well as hollow and porous features possess improved performance with respect to electrocatalytic activity (2.72 mA/cm^2 at peak potential, which is 2.1 times greater than that of Pt black) and durability toward methanol oxidation.

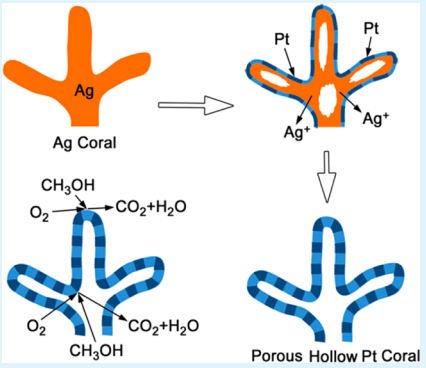

KEYWORDS: *platinum, coral-like, hollow mesocrystal, porous structure, electrocatalytic, methanol oxidation*

1. INTRODUCTION

Platinum nanomaterials are excellent catalysts for a number of reactions, including the industrial synthesis of nitric acid, reduction of pollutant gases, oil cracking, proton exchange membrane (PEM) fuel cells, etc.[1] At present, the most widely used Pt catalyst consists of small nanoparticles (2−5 nm) that have a large surface area or large polyhedral structures with high-index facets to enhance surface reaction activity.[2,3] The main problem associated with the supported Pt nanoparticle catalysts is the significant loss of electrochemical surface area (ECSA) and, thus, the degradation of catalytic performance caused by Pt nanoparticle migration, coalescence, or even detachment from the catalyst system. In addition, Ostwald ripening of the Pt nanoparticles could occur because of their high surface energy and zero-dimensional structural features.[4] Therefore, our main challenge is the simultaneous realization of highly active and highly durable catalyst.

Several strategies for improving the durability of Pt-based catalysts against the loss of ECSA have been developed, including alloying protocols such as Pt−Pd, Pt−Au, Pt−Ni, Pt−Co, and Pt−Fe and various structures such as one-dimensional Pt nanostructures, two-dimensional macroscopic membranes, and three-dimensional nanostructures.[5−12] In this paper, the application of mesostructures for improving the durability of a catalyst will be highlighted. This proposal partially results from the fact that mesocrystals demonstrate some intrinsic advantages such as a rough surface, a high internal porosity, the small size of the building block, a single-crystal structure, and high densities of crystalline defects,[13−16] which all may contribute to high activity.[17] Furthermore, some previous studies have also implied that mesostructures with single-crystal features have a promising stability in an electrochemical reaction. This is because the larger porous mesoparticles with a single-crystal structure are more stable than small nanoparticles during the electrochemical reaction.[5] For example, Qi et al. reported unique spindle-shaped nanoporous anatase TiO_2 mesocrystals. Because of their intrinsic single-crystal-like nature, as well as the high porosity of the nanoporous mesostructures, the products exhibited remarkable crystalline-phase stability and improved performance as anode materials for lithium ion batteries.[18] In addition, Zheng et al. synthesized mesocrystalline Pd nanocorolla via a surface-confined etching growth process. Because of the presence of internal voids and an increased apparent thickness, the Pd mesocrystals also demonstrated several features superior to the single-domain Pd nanosheets.[19]

In previous studies, nanoparticle-aggregated nanostructures for use as electrocatalysts, e.g., Pd−Pt bimetallic nanodendrities, as reported by Xia and other groups, were much more active than the state-of-the-art Pt/C catalyst because of their relatively large surface areas.[5,20−22] However, the durability could still be improved because of the presence of nanostructures with a size of ~50 nm resulting in the reduction of ECSA loss. If one can design a structure at the meso- or macroscale that demonstrates a large surface area and simultaneously high electrochemical activity, then durability would probably be achieved. Recently, well-controlled mesoporous single-crystal Pt has been synthesized using a hard-template strategy; however, the catalytic properties have not been studied.[23] In this paper, on the basis of our previous experience in synthesizing a variety of hierarchically structured

Received: September 25, 2012
Accepted: November 23, 2012
Published: November 23, 2012

mesocrystals,[24−28] we report a new type of hollow coral-like mesostructural Pt catalyst with simultaneously high electrochemical activity and improved durability. The Pt mesocrystals were synthesized via a facile replacement process with hierarchically structured Ag nanoparticles as the template. The microstructures of hollow coral-like Pt mesocrystals and their electrocatalytic properties toward methanol oxidation were investigated in detail. The obtained Pt mesocrystals possess unique structural features, such as a hollow interior and a porous nature; thus, they exhibit remarkable electrocatalytic activity. Importantly, the single-crystal-like structure of the Pt mesocrystals, which consists of a great number of nanoparticle building units (~5 nm), results in them demonstrating an improved durability during electrochemical oxidation of methanol. Additionally, this synthetic protocol will also be employed to obtain various components, such as Pd- and Pt-based alloy catalysts.

2. EXPERIMENTAL SECTION

2.1. Materials. Silver nitrate ($AgNO_3$), ascorbic acid, and chloroplatinic acid hexahydrate ($H_2PtCl_6{\cdot}6H_2O$) were all analytical grade and used as received. Deionized water (Millipore) was used in all preparations. The ascorbic acid solutions were freshly prepared before they were used.

2.2. Synthesis of Coral-like Ag Particles. In a typical synthesis, 0.25 mL of a 20 mM aqueous $AgNO_3$ solution was added to 8.5 mL of deionized water, followed immediately by the addition of 1.25 mL of a 100 mM aqueous ascorbic acid solution. The reaction was conducted at room temperature without stirring. The initially colorless $AgNO_3$ solution turned light gray within 5 s of the addition of the ascorbic acid solution; after 20 min, it did not become any darker. The gray products were isolated after 12 h by consecutive washing−centrifugation cycles with ethanol and deionized (DI) water. They were subsequently dried for 6 h in air at room temperature for further use.

2.3. Synthesis of Hollow Coral-like Pt Mesocrystals. The as-synthesized sliver particles were redispersed into 20 mL of DI water assisted by ultrasonic vibration. Then, 2 mL of a 10 mM aqueous H_2PtCl_6 solution was added. The initially light gray Ag suspension turned black immediately. After 2 h, l0 mL of ammonia (25%) was added. The mixture was aged for more than 3 h to complete the dissolution of AgCl, followed by filtering and consecutive washing−centrifugation cycles with ethanol and DI water. Afterward, the product was dispersed in 10 mL of a 2 M cold nitric acid aqueous solution for aging for 96 h. Finally, the black products were obtained by filtering and further consecutive washing−centrifugation cycles with ethanol and DI water.

2.4. Structural Characterization. The morphology of the silver and platinum nanostructures was observed by field-emission scanning electron microscopy (FE-SEM, JEOL JSM-7000F) and transmission electron microscopy (TEM, JEOL JEM-2100). The chemical composition and purity of the products were examined by electron energy dispersive X-ray (EDX) analysis. Their crystalline structures were characterized with an X-ray diffractometer (Bruker-AXS D8 ADVANCE) using Cu Kα radiation (λ = 1.5405 Å) in the range of 30−90°. The samples were prepared by depositing a drop of an aqueous suspension of particles on a piece of silicon wafer (for SEM) or a carbon-coated copper grid (for TEM) and dried at room temperature.

2.5. Electrochemical Measurements. Cyclic voltammogram (CV) experiments were performed using an electrochemical analyzer. A conventional three-electrode cell was used, including a Ag/AgCl (saturated KCl) electrode as the reference electrode, a platinum wire as the counter electrode, and a glassy carbon electrode (GCE) (5 mm in diameter) as the working electrode. The GCE was carefully polished and washed before every experiment. First, 4.9 mg of the product was dispersed in a mixture of DI water and 2-propanol ($V_{water}/V_{2\text{-propanol}}$ = 4/1) at a concentration for 1.0 mg/mL metal catalyst solvent, followed by sonication of 10 min. A stream of air was used to dry the mixture after it was deposited on the GCE. The amount of metal deposited on the GCE was 8 μg, which was same as that in ref 20. After evaporation of the water and 2-propanol in air, 8 μL of a 0.025 wt % Nafion solution was dropped on the electrode surface to attach the catalyst to the glassy carbon.

Electrochemical properties were measured on a CHI 760 dual-channel electrochemical working station. Hydrogen adsorption−desorption CVs were recorded in a nitrogen-protected 0.1 M perchloric acid ($HClO_4$) aqueous solution with a scanning rate of 50 mV/s. The solution was purged with N_2 for 30 min to remove the dissolved O_2 before measurements were taken. The region for hydrogen adsorption (0.2604−0.1096 V on the backward potential scan) was used to estimate the ECSAs. For the methanol oxidation reaction, a nitrogen-saturated aqueous solution containing 0.5 M methanol and 0.1 M perchloric acid was used. The voltage region of the cyclic voltammograms and chronoamperograms was from −0.2904 to 0.909, and the current densities in cyclic voltammograms were applied to evaluate the catalytic current. All of the experiments were conducted at room temperature (25 °C).

3. RESULTS AND DISCUSSION

3.1. Morphology and Structural Characteristics of Coral-like Pt Mesocrystals. To prepare hollow coral-like Pt nanoparticles, coral-like Ag nanoparticles were first synthesized using a facile protocol. As shown in Figure 1a, the coral-like Ag

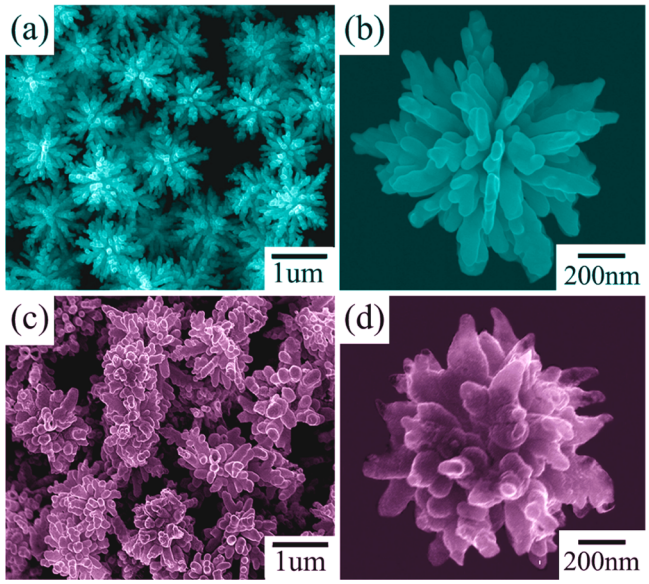

Figure 1. (a) Low-magnification and (b) high-magnification SEM images of Ag corals. (c) Low-magnification and (d) high-magnification SEM images of Pt corals, which were synthesized using as-prepared Ag corals (as shown in panels a and b) as the sacrificial template.

nanoparticles were well controlled and uniformly dispersed. Individual Ag corals had a narrow size distribution, with the average size being around 1.5 μm. The microstructure of the coral-like Ag mesoparticles may be observed from the high-magnification image shown in Figure 1b, demonstrating a symmetrical structure that is composed of trunks and irregular secondary nanobranches. Using Ag corals as the template, well-defined hollow coral-like Pt mesostructures were synthesized via a facile replacement process as shown in panels c and d of Figure 1. One can observe that the as-prepared Pt coral-like mesoparticles display a size and a morphology similar to those of the coral-like Ag template. Some partially broken tips in

Figure 1d show the hollow interior, which indicates the formation of hollow Pt mesocorals.

The morphology and interior structure of the coral-like Pt mesostructures were further investigated by TEM and selected area electron diffraction (SAED) patterns. Panels a and b of Figure 2 show that the coral-like Pt mesostructures have a

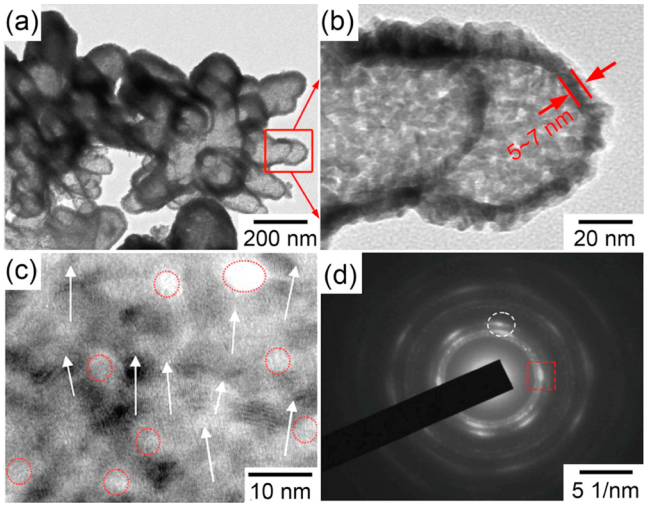

Figure 2. (a) TEM image of Pt corals and (b) a single branch of a Pt coral (the wall thickness where marked is around 5−7 nm). (c) HRTEM images of the branch in panel b and pores identified by the circles and (d) corresponding SAED pattern for the whole branch as shown in panel b, where the red box and white circle indicate the single-crystal-like SAED feature.

coral-like morphology that is the same as that of the Ag template and a strong contrast difference between their edges (dark) and center (bright), which indicates the Pt mesostructures possess a hollow interior. This can also be clearly observed from Figure 2b, where the wall thickness of the hollow Pt mesostructures is 5−7 nm. If the TEM image is further magnified, one can note that the hollow Pt mesocorals consist of a large number of Pt nanoparticles with a size of ∼5 nm and pores with a size of ∼2 nm, indicated by red circles in Figure 2c. Interestingly, as the SAED pattern is shown in Figure 2d and was recorded from the whole branch of the Pt mesostructure in Figure 2b, it displays a single-crystal structure with a certain degree of imperfect crystallographic orientation. The discontinuous diffraction spots suggest that a large amount of the Pt nanoparticles share common crystallographic orientations, as indicated by the arrows in Figure 2c. This structure, which is a feature of a mesocrystal, is called an imperfect single crystal.[13−15] Similar to other mesocrystal growth,[29] a large amount of Pt nanoparticles that acted as building units during the growth aggregated through self-assembly to form the mesocrystal. During this particle-mediated growth, the particle unit shared the same crystallographic orientation through an OA (oriented attachment) mechanism.[16,29]

The chemical composition of the Pt mesostructures was determined by EDX analysis, and the details are listed in Table 1. The carbon element in the EDX came from conductive tape, which was mainly composed of carbon black and was used to support the sample in the EDX measurement. The results of EDX analysis showed that the mesostructures were mainly composed of the Pt element; the residual Ag element was no

Table 1. Results of EDX Analysis of Hollow of Pt Mesocorals and Hollow Pt Mesocages

		C	Ag	Pt	total
weight percent (%)	Pt mesocorals	1.25	4.68	94.07	100
	Pt mesocages	0.46	4.74	94.8	100

more than 5%. Figure 3 shows the powder X-ray diffraction (PXRD) patterns of the Ag coral-like template mesoparticles

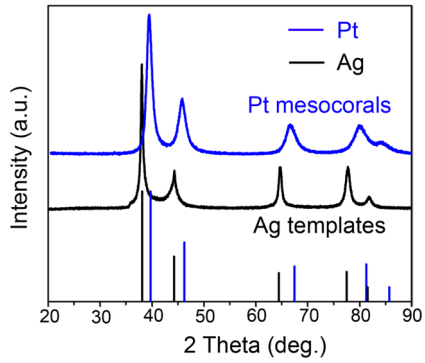

Figure 3. PXRD patterns of Ag coral-like templates and Pt mesocorals.

and Pt mesostructures. The diffraction pattern of the Ag template could be readily indexed to (111), (200), (220), (311), and (222) planes of the pure fcc (face-centered cubic) Ag lattice (87-0719, JCPDS-ICDD). The PXRD patterns of the Pt mesostructures could all be indexed to (111), (200), (220), (311), and (222) diffractions of a fcc structure, with the peak positions very near the pure fcc Pt metal (70-2057, JCPDS-ICDD); for instance, the (111) peak position of the Pt mesostructure was 39.5° (2θ) and the standard (111) peak position of pure fcc Pt metal 39.8° (2θ). The fact that no Ag diffraction patterns were observed and there was very little left shift of the peaks, when compared to Pt metal, indicates that residual Ag atoms [<5% weight (Table 1)] diffused into the Pt metal and a solid solution alloy phase was formed. Calculated using the Scherrer formula, the average crystal size of Pt mesostructures was around 9 nm and that of Ag templates was 26 nm.

The analysis presented above not only indicates that the center of the Pt coral is hollow but also shows that the shell of the hollow coral is porous. This hollow and porous structure supplies a large active surface for the electrochemical catalyst. The electrochemical catalytic properties of the Pt hollow corals were studied, using the methanol oxidation reaction (MOR) system. To evaluate the influence of the morphology, of the hollow Pt corals, on catalytic activity, the properties of the Pt spherical mesocages and commercial Pt blacks were measured for comparison. Similar to the synthesis of the hollow Pt corals, the spherical Pt hollow mesocages were synthesized using spherical meatball-like Ag particles as the sacrificial template (shown in Figure 4a). Similar to the hollow Pt corals, the spherical Pt mesocages also show a hollow and porous structure, as shown in panels b and c of Figure 4. The difference is that there are no branches on the particles and the walls are probably thicker than the Pt hollow corals, indicating that the surface area per mass is smaller than that of the Pt hollow corals. The EDX spectrum is shown in Figure 4d, and a certain degree of residual Ag can be observed in the product.

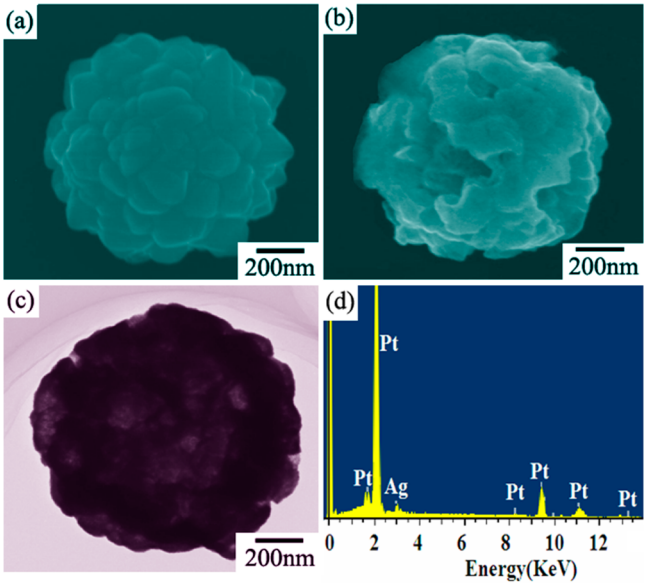

Figure 4. SEM images of (a) a single spherical Ag particle and (b) a single spherical Pt mesocage. (c) TEM image of a single spherical Pt mesocage. (d) EDX spectrum of Pt mesocages.

3.2. Elecctrochemical Properties of Coral-like Pt Mesocrystals. Figure 5a shows CV curves of the three catalysts recorded at room temperature in an argon gas-purged 0.1 M $HClO_4$ solution at a scan rate of 50 mV/s. ECSAs were calculated by measuring the charge collections of hydrogen adsorption on Pt assuming a value of 210 $\mu C/cm^2$ for the adsorption of a hydrogen monolayer. ECSAs of the hollow Pt corals were the largest (22.3 m^2/g) compared with those of Pt spherical mesocages (16.5 m^2/g) and commercial Pt blacks (19.4 m^2/g). The relatively large ECSAs of Pt mesocorals may be due to their intrinsic structure, consisting of a hollow interior, small ~5 nm nanoparticles, and abundant ~2 nm pores.

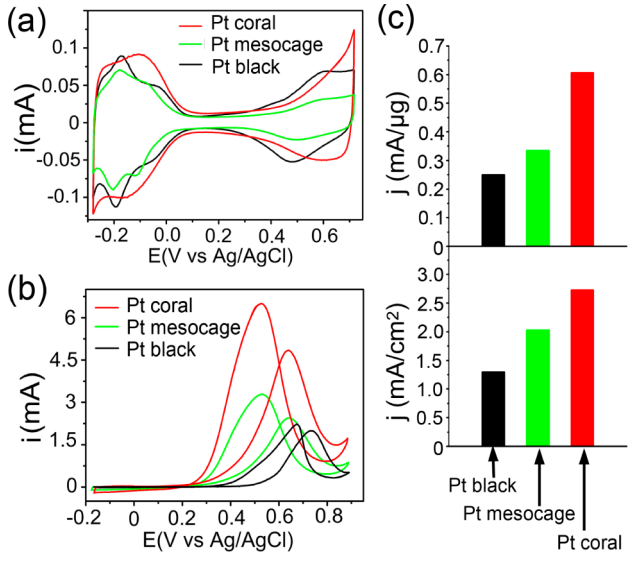

Figure 5. (a) CV profiles of Pt blacks, Pt corals, and Pt spheres in a 0.1 M $HClO_4$ solution at room temperature. (b) CVs of MOR on Pt blacks, Pt corals, and Pt spheres as catalysts in 0.1 M $HClO_4$ and 0.5 M CH_3OH. (c) Comparison of peak specific area currents and peak specific mass currents of Pt blacks, Pt corals, and Pt spheres at a potential of 0.7 V vs Ag/AgCl. All scanning rates were 50 mV/s.

The electrocatalytic measurement of the three catalysts was performed in an argon gas-purged 0.1 M $HClO_4$/0.5 M CH_3OH solution using a glassy carbon rotating disk electrode (RDE) at room temperature with a scan rate of 50 mV/s. The CV curves of MOR on the three catalysts are shown in Figure 5b, which demonstrate little difference in the shape among these three catalysts, suggesting a similar reaction pathway.[30] The onset and peak potentials of hollow Pt corals are the same as those of Pt spherical mesocages and lower than those of Pt black, suggesting a lower potential for methanol and carbon monoxide oxidation on hollow Pt corals. According to the comparison of peak specific activity, the hollow Pt corals exhibit the highest activity of 2.72 mA/cm^2 at their peak potential of 0.659 V, which is 2.1 times greater than that of Pt black (1.29 mA/cm^2). For the Pt spherical mesocages, the peak specific area current was 2.02 mA/cm^2, which is 25.7% lower than that of the Pt corals (Figure 5c). On the basis of the normalized peak current against the ECSA of each catalyst, the hollow Pt corals have a peak mass specific activity that is 2.42 times that of Pt black and 1.81 times that of the Pt spherical mesocages. Compared with mesoporous Pt catalysts in other reports,[30,31] the Pt corals show greatly improved catalytic activity.

The rate of surface poisoning of the three catalysts was evaluated using chronoamperometry in a 0.1 M $HClO_4$/0.5 M CH_3OH solution at a constant potential of 0.65 V for 4000 s. The results are shown in Figure 6. The polarization currents for all the obtained catalysts decrease rapidly during the early stage, because of the formation of intermediate species during MOR. However, the current decreasing rate for coral-like Pt mesocrystals was slower than those for the other two catalysts. In the first 1000 s, the current of the Pt coral decreased to 50% and those of the Pt mesocage and Pt black decreased to 20 and 27%, respectively. In the whole range of 4000 s, the current of the Pt coral decreased to 21% and those of the Pt mesocage and Pt black decreased to 15 and 12%, respectively. As in the report of Yamauchi and Franceschini,[21,30] the lagged decreasing rate and the highest current during the whole process (~4000 s) were seen for the coral-like Pt mesocrystals, indicating that the electrocatalytic stability of the hollow Pt corals for MOR was higher than that of Pt black and Pt spherical mesocages.

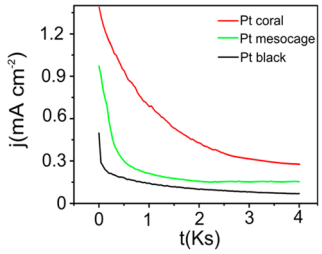

Figure 6. Chronoamperometric response of oxidation of 0.5 M methanol in a 0.1 M $HClO_4$ solution at a constant potential of 0.65 V.

As shown in Scheme 1, using the Ag coral-like particles as templates, Pt metal continuously grew on the particle surface along with the disappearing Ag atoms. Stabilized by Pt atoms, the Ag atoms near the surface were more stable than those located at the particle center. Thus, the Ag atoms in the particle center were first dissolved as Ag ions. Finally, most of the Ag atoms were replaced with Pt atoms through a replacement reaction, and the hollow Pt mesostructures were formed. The

Scheme 1. (a–c) Illustrations of the Synthesis Route of Porous Pt Mesocrystals Using Coral-like Ag Nanoparticles as the Sacrificial Template and (d) Hollow and Porous Structures of Pt Mesocrystals That Improve the Catalytic Properties for Methanol Oxidation

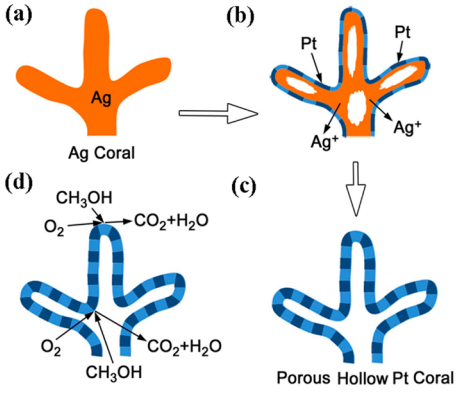

remaining Ag atoms mixed with the Pt atoms to form the solid solution alloy phase because of the disappearance of the miscibility gaps for the Ag and Pt metals in nanostructured alloys.[16,32,33] Most similar to hollow metal nanoparticles prepared via a sacrificial template,[26,34,35] the walls of the Pt hollow corals are porous. The hollow and porous structure, as shown in Scheme 1d, possesses great advantages for catalytic applications because of the catalytic reaction for MOR that can be conducted both outside and inside the porous walls. Compared with Pt black and Pt spherical mesocages, the special structure and morphology of the hollow coral-like Pt mesocrystals, consisting of large active points formed at multibranched tips, corners, and pores on the surface, potentially improve the catalytic performance. In addition, the electrocatalytic properties can be improved by the lattice distortion in the mesocrystals.[36,37] As previously reported, during mesocrystal growth, the crystalline directions of the nanoparticle units did not match very well with each other.[29] Thus, lattice distortion was introduced into the mesocrystal. On the other hand, the large size of the whole hollow coral-like Pt mesoparticle promotes the stability resulting from the mesocrystal crystalline nature.[5]

3.3. Influence of Residual Ag on Electrochemical Properties. During the formation of Pt atoms via the replacement reaction, Ag atoms may mix with Pt atoms thus forming PtAg alloys. To minimize the amount of residual Ag in the Pt hollow coral-like mesocrystals, acid treatment was conducted. The influence of residual Ag on the electrochemical catalytic properties was investigated. Three samples with different Ag composition ratios were prepared by controlling the acid treatment time. Samples with 25, 18.8, and 4.7% Ag composition ratios were obtained after acid treatment for 4, 24, and 96 h, respectively. During the acid treatment, the surface Ag atoms were first removed by oxidation; thus, a core–shell structure was formed during the acid treatment as described in the literature,[38,39] where Ag atoms around the surface region were removed and those in the center of the hollow coral walls were not removed and their composition ratio was kept unchanged.

The metal Ag has no catalytic properties for MOR. The catalytic properties of the Pt atoms are suppressed when the Ag atoms form an alloy with them. However, it was found that the Pt@Ag core–shell structures improved the catalytic properties for the FAOR (formic acid oxidation reaction).[38] In this experiment, the catalytic properties of the hollow corals with 25, 18.8, and 4.7% Ag compositions for MOR were measured, and the comparison is shown in Figure 7. The ECSAs increased

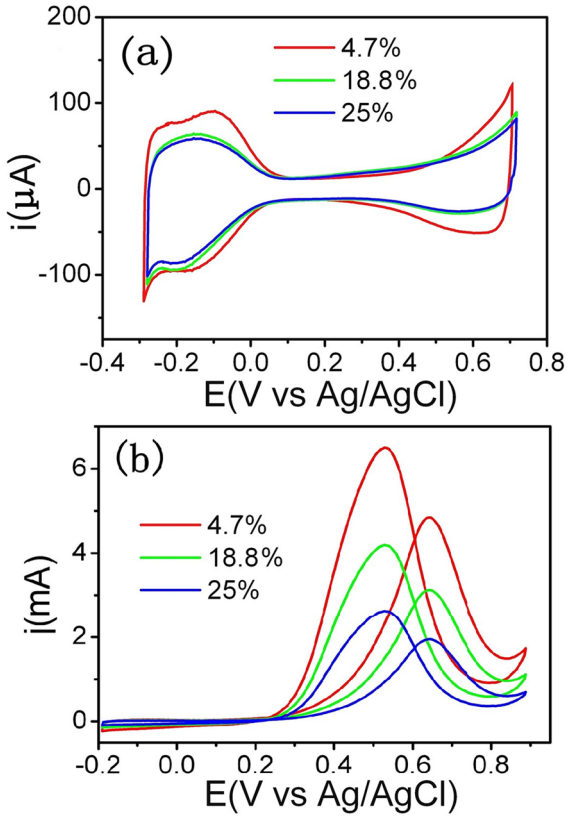

Figure 7. (a) CV profiles of Pt corals with different Ag residual contents in a 0.1 M $HClO_4$ solution at room temperature. (b) CVs of MOR on Pt corals with different Ag residual contents in 0.1 M $HClO_4$ and 0.5 M CH_3OH.

as the Ag composition decreased, as shown in Figure 7a, indicating that the wall thickness of the hollow corals decreased when the Ag element was removed. When the Ag composition decreased from 25 to 4.7%, the ECSAs increased from 18.7 to 22.3 m^2/g. Figure 7b shows the CV curves of the three samples for MOR catalysis at the same mass. It is shown that the sample with 4.7% Ag possesses the highest catalytic properties. The peak current of the catalytic reaction for the sample with 4.7% Ag was 5.16 mA, nearly 1.8 and 2.6 times those for the samples with 25 and 18.8% Ag, respectively. When the composition of the Ag element decreased from 25 to 4.7%, the peak positions of the current curve shift from 0.685 to 0.639 V and the start points for the current peaks decreased from 0.32 to 0.19 V. From this, it can be seen that the highest catalytic activity was exhibited by the sample with 4.7% Ag.

According to the experimental results described above, the specific electric catalytic activities of the PtAg hollow corals strongly depend on the surface electronic and geometric structures of the PtAg nanoalloys. The mixed Ag atoms in the PtAg alloy should promote the catalytic activity of the Pt atoms by altering the electronic structures. The electron cloud of Ag atoms will shift to Pt atoms, and the correlated d-band center for PtAg shifts upward in comparison with pure Pt.[40,41] However, in this experiment, the catalytic properties of PtAg hollow corals, before acid treatment, were suppressed by Ag

atoms. This is probably due to the fact that the segregation of Ag atoms can be favorable on the surface of the PtAg alloy, which results in a large decrease in the number of neighboring Pt atoms.[42,43] Thus, the reduction in the number of adsorption sites for poisoning species slows the electrocatalytic reactions in MOR.[43−46] As the Ag atoms in the surface region are removed, the surface of the hollow corals becomes Pt-rich and the residual Ag atoms are imbedded below the Pt surface. In this situation, the catalytic properties of Pt atoms on the surface are promoted by imbedded Ag atoms. On the other hand, the lattice distortions induced by mismatched Pt and Ag atoms may also promote catalytic activity.[39]

4. CONCLUSIONS

In summary, by means of the replacement reaction between Ag and H_2PtCl_4, well-defined hollow coral-like Pt mesostructures have been prepared simply at room temperature with Ag corals as sacrificial templates. The morphology, structure, composition, and electrochemical properties have been characterized for hollow Pt mesocrystals under various types of Ag doping. It has been demonstrated that hollow coral-like Pt mesocrystals exhibit an enhanced catalytic performance for methanol oxidation because of their special structure and morphology. When only considering the catalytic properties of Pt mesostructures, they show considerable potential to be used in direct methanol fuel cells, as they are low-cost and highly efficient catalysts. This simple synthetic protocol can potentially be extended to the fabrication of hollow noble metal materials and their alloy-based electrocatalysts for fuel cells.

AUTHOR INFORMATION

Corresponding Author

*E-mail: hjyou@mail.xjtu.edu.cn (H.Y.) or jxfang@mail.xjtu.edu.cn (J.F.).

Notes

The authors declare no competing financial interest.

ACKNOWLEDGMENTS

This work was supported by the National Natural Science Foundation of China (Grants 51171139, 50901056, and 51201122), the Natural Science Foundation of Shaanxi Province (Grant 2012JQ6006), the Tengfei Talent Project of Xi'an Jiaotong University, New Century Excellent Talents in University (NCET), the Doctoral Fund for New Teachers (20110201120039), the Scientific New Star Program in Shann Xi Province (2012KJXX-03), and Fundamental Research Funds for the Central Universities (08142008).

REFERENCES

(1) Chen, J. Y.; Lim, B.; Lee, E. P.; Xia, Y. N. *Nano Today* **2009**, *4*, 81−95.
(2) Ahmadi, T. S.; Wang, Z. L.; Green, T. C.; Henglein, A.; El Sayed, M. A. *Science* **1996**, *272*, 1924−1926.
(3) Tian, N.; Zhou, Z.-Y.; Sun, S.-G.; Ding, Y.; Wang, Z. L. *Science* **2007**, *316*, 732−735.
(4) Joo, S. H.; Choi, S. J.; Oh, I.; Kwak, J.; Liu, Z.; Terasaki, O.; Ryoo, R. *Nature* **2001**, *412*, 169−172.
(5) Peng, Z.; Yang, H. *J. Am. Chem. Soc.* **2009**, *131*, 7542−7543.
(6) Kim, Y.; Hong, J. W.; Lee, Y. W.; Kim, M.; Kim, D.; Yun, W. S.; Han, S. W. *Angew. Chem., Int. Ed.* **2010**, *49*, 10197−10201.
(7) Wu, J. B.; Qi, L.; You, H. J.; Gross, A.; Li, J.; Yang, H. *J. Am. Chem. Soc.* **2012**, *134*, 11880−11883.
(8) Yang, H.; Zhang, J.; Sun, K.; Zou, S.; Fang, J. *Angew. Chem., Int. Ed.* **2010**, *49*, 6848−6851.
(9) Liang, H.-W.; Cao, X.; Zhou, F.; Cui, C.-H.; Zhang, W.-J.; Yu, S.-H. *Adv. Mater.* **2011**, *23*, 1467−1471.
(10) Song, Y. J.; Yang, Y.; Medforth, C. J.; Pereira, E.; Singh, A. K.; Xu, H. F.; Jiang, Y. B.; Brinker, C. J.; van Swol, F.; Shelnutt, J. A. *J. Am. Chem. Soc.* **2004**, *126*, 635−645.
(11) Lim, B.; Lu, X.; Jiang, M.; Camargo, P. H. C.; Cho, E. C.; Lee, E. P.; Xia, Y. *Nano Lett.* **2008**, *8*, 4043−4047.
(12) Zhang, L.; Li, N.; Gao, F.; Hou, L.; Xu, Z. *J. Am. Chem. Soc.* **2012**, *134*, 11326−11329.
(13) Fang, J.; Ding, B.; Gleiter, H. *Chem. Soc. Rev.* **2011**, *40*, 5347−5360.
(14) Zhou, L.; O'Brien, P. *Small* **2008**, *4*, 1566−1574.
(15) Song, R. Q.; Colfen, H. *Adv. Mater.* **2010**, *22*, 1301−1330.
(16) Fang, J.; You, H.; Kong, P.; Yi, Y.; Song, X.; Ding, B. *Cryst. Growth Des.* **2007**, *7*, 2674−2676.
(17) Zhou, L.; O'Brien, P. *J. Phys. Chem. Lett.* **2012**, *3*, 620−628.
(18) Ye, J.; Liu, W.; Cai, J.; Chen, S.; Zhao, X.; Zhou, H.; Qi, L. *J. Am. Chem. Soc.* **2011**, *133*, 933−940.
(19) Huang, X.; Tang, S.; Yang, J.; Tan, Y.; Zheng, N. *J. Am. Chem. Soc.* **2011**, *133*, 15946−15949.
(20) Lim, B.; Jiang, M.; Camargo, P. H. C.; Cho, E. C.; Tao, J.; Lu, X.; Zhu, Y.; Xia, Y. *Science* **2009**, *324*, 1302−1305.
(21) Wang, L.; Nemoto, Y.; Yamauchi, Y. *J. Am. Chem. Soc.* **2011**, *133*, 9674−9677.
(22) Wang, L.; Yamauchi, Y. *J. Am. Chem. Soc.* **2010**, *132*, 13636−13638.
(23) Wang, H. J.; Jeong, H. Y.; Imura, M.; Wang, L.; Radhakrishnan, L.; Fujita, N.; Castle, T.; Terasaki, O.; Yamauchi, Y. *J. Am. Chem. Soc.* **2011**, *133*, 14526−14529.
(24) Fang, J.; Leufke, P. M.; Kruk, R.; Wang, D.; Scherer, T.; Hahn, H. *Nano Today* **2010**, *5*, 175−182.
(25) Fang, J.; Du, S.; Lebedkin, S.; Li, Z.; Kruk, R.; Kappes, M.; Hahn, H. *Nano Lett.* **2010**, *10*, 5006−5013.
(26) Hong, F.; Sun, S.; You, H.; Yang, S.; Fang, J.; Guo, S.; Yang, Z.; Ding, B.; Song, X. *Cryst. Growth Des.* **2011**, *11*, 3694−3697.
(27) You, H.; Ji, Y.; Wang, L.; Yang, S.; Yang, Z.; Fang, J.; Song, X.; Ding, B. *J. Mater. Chem.* **2012**, *22*, 1998−2006.
(28) Fang, J.; Ding, B.; Song, X. *Cryst. Growth Des.* **2008**, *8*, 3616−3622.
(29) You, H. J.; Chen, F.; Yang, S. C.; Yang, Z. M.; Ding, B. J.; Liang, S. H.; Song, X. P. *Cryst. Growth Des.* **2011**, *11*, 5449−5456.
(30) Franceschini, E. A.; Planes, G. A.; Williams, F. J.; Soler-Illia, G.; Corti, H. R. *J. Power Sources* **2011**, *196*, 1723−1729.
(31) Planes, G. A.; Garcia, G.; Pastor, E. *Electrochem. Commun.* **2007**, *9*, 839−844.
(32) Peng, Z.; You, H.; Yang, H. *ACS Nano* **2010**, *4*, 1501−1510.
(33) Peng, Z.; Yang, H. *J. Solid State Chem.* **2008**, *181*, 1546−1551.
(34) Fang, J.; Lebedkin, S.; Yang, S.; Hahn, H. *Chem. Commun.* **2011**, *47*, 5157−5159.
(35) Zeng, J.; Zhang, Q.; Chen, J.; Xia, Y. *Nano Lett.* **2010**, *10*, 30−35.
(36) You, H. J.; Peng, Z. M.; Wu, J. B.; Yang, H. *Chem. Commun.* **2011**, *47*, 12595−12597.
(37) Wu, J. B.; Qi, L.; You, H. J.; Gross, A.; Li, J.; Yang, H. *J. Am. Chem. Soc.* **2012**, *134*, 11880−11883.
(38) Peng, Z.; You, H.; Yang, H. *Adv. Funct. Mater.* **2010**, *20*, 3734−3741.
(39) Yang, H. *Angew. Chem., Int. Ed.* **2011**, *50*, 2674−2676.
(40) Ruban, A.; Hammer, B.; Stoltze, P.; Skriver, H. L.; Norskov, J. K. *J. Mol. Catal. A: Chem.* **1997**, *115*, 421−429.
(41) Hammer, B.; Norskov, J. K. Theoretical Surface Science and Catalysis: Calculations and Concepts. In *Advances in Catalysis, Volume 45: Impact of Surface Science on Catalysis*; Gates, B. C., Knozinger, H., Eds.; Academic Press Inc.: San Diego, 2000; Vol. *45*, pp 71−129.
(42) Greeley, J.; Norskov, J. K.; Mavrikakis, M. *Annu. Rev. Phys. Chem.* **2002**, *53*, 319−348.
(43) Demirci, U. B. *J. Power Sources* **2007**, *173*, 11−18.

(44) Xu, J. B.; Zhao, T. S.; Liang, Z. X. *J. Phys. Chem. C* **2008**, *112*, 17362−17367.
(45) Choi, J. H.; Jeong, K. J.; Dong, Y.; Han, J.; Lim, T. H.; Lee, J. S.; Sung, Y. E. *J. Power Sources* **2006**, *163*, 71−75.
(46) Yu, X. W.; Pickup, P. G. *J. Power Sources* **2008**, *182*, 124−132.

NOTE ADDED AFTER ASAP PUBLICATION

This paper was originally published on the Web on December 5, 2012, with a different version of Figure 2. The revised version was reposted on December 26, 2012.